Properties and nature of Be stars

XVIII. Spectral, light and colour variations of 4 Herculis[⋆,⋆⋆]

P. Koubský[1], P. Harmanec[1], J. Kubát[1], A.-M. Hubert[2], H. Božić[3], M. Floquet[2], P. Hadrava[1], G. Hill[4], and J.R. Percy[5]

[1] Astronomický ústav, Akademie věd České republiky, 251 65 Ondřejov, Czech Republic
[2] Observatoire de Paris, Section d'Astrophysique de Meudon, URA 335 du CNRS, F-92195 Meudon Cedex, France
[3] Faculty of Geodesy, University of Zagreb, Kačićeva 26, 41000 Zagreb, Croatia
[4] Department of Physics, University of Auckland, 38 Princess Street, Auckland, New Zealand
[5] Erindale Campus, University of Toronto, Mississauga, Ontario L5L 1C6, Canada

Abstract. An analysis of a rich series of spectroscopic and photometric observations of the Be star 4 Her led to the following conclusions:

– 4 Her is another example of a long-term Be variable with a type of correlation between the brightness and emission strength, similar to 88 Her (V744 Her) and BU Tau (Pleione). It is argued that the formation of a new Be envelope of 4 Her starts with the creation of a slightly cooler pseudophotosphere at the equatorial regions of the star (seen under some intermediate inclination angle) which only gradually grows into an optically thin extended envelope.

– Radial-velocity measurements of the centre of the Hα emission and of the photospheric lines confirm the binary nature of the star. The first reliable orbital elements are presented. The 46-d orbit is nearly circular and has a semiamplitude of $5-8\,\mathrm{km\,s^{-1}}$. An LTE model atmosphere analysis of the photospheric spectrum of the primary leads to T_{eff} = 12500K, $\log g$ = 4.0, and $v\sin i$ = 300 km s^{-1}. No direct evidence of the low-mass secondary was found and the possibility that the secondary fills its Roche lobe can be safely excluded.

– The central quasi-emission bumps (CQEB) visible as "doubling" of some shell lines appear during the phase of the formation of a new shell. They are strongest during the light minimum and become fainter as the Hα emission strengthens.

– An unusual blue-shifted absorption component of the Hα line, never reported before, re-appears strictly periodically in the V peak of the Hα emission at a limited range of velocities and orbital phases.

– It is argued that the observational facts about 4 Her are probably best reconciled by a model which assumes that the secondary is a hot and rotationally unstable object which looses mass towards the primary via a gas stream. However, some important findings remain unexplained.

Key words: stars: binaries: spectroscopic – stars: emission-line, Be – stars: variable – stars: individual: 4 Her

1. Introduction

4 Herculis (V839 Her, HD 142926, HR 5938, SAO 45970, BD +42°2652; V = 5$^{\mathrm{m}}$75, $v\sin i$ = 350 km s^{-1}, according to the *Bright Star Catalogue*) is a well known and rather frequently observed Be and shell star. It was recognized as a Be star by Heard (1939) and Mohler (1940). The estimates of the spectral type of 4 Her by different authors vary between B7 IV-V and B9e. Hubert (1971), Harmanec et al. (1976, P6 hereafter), Hubert-Delplace & Hubert (1979) and Koubský et al. (1994) give descriptions of long-term variations in the optical spectrum of 4 Her. As in some other Be stars, the variations are characterized by disappearance and subsequent re-appearance of the Hα emission. According to Koubský et al. (1994), the length of both emission and non-emission cycles varies between 3 and 20 years in the case of 4 Her. In the same paper, a positive correlation between the strength of the Hα emission and central intensity of the C IV doublet at 1548 and 1551 Å (based on IUE spectra taken in 1979, 1983 and 1992) was found. The onset of a recent shell phase of 4 Her was announced by Koubský et al. (1993).

Plaskett et al. (1922) reported 4 Her to be a spectroscopic binary. Later, Heard (1940) found periodic radial-velocity (RV hereafter) variations of the star with a period of 0$^{\mathrm{d}}$97625. Harmanec et al. (1973, P3 hereafter) showed that the RV period

obtained by Heard (1940) was in fact a one-day alias of the true period of 46 days. They, therefore, revived the idea that the object is a single-line spectroscopic binary. The elements of the system were later refined by Heard et al. (1975, P5 hereafter) to $P = 46^d194$, $K = 12$ km s^{-1} and $e = 0.3$. P6 studied the RV variations of emission and absorption components of the hydrogen lines. They concluded that the observed eccentricity of the orbit was spurious, caused by the effects of circumstellar matter in the interacting binary system. This conclusion was reinforced by Koubský et al. (1994) who measured the RVs of hydrogen profiles on spectra taken during two epochs when the lines were *without* shell components. They arrived at a circular orbit with an amplitude lower than that derived earlier from the shell lines.

The suspicion that 4 Her is an interacting binary led several authors to systematic UBV observations of the star. However, no orbital light variations were found (Hill et al. 1976, Landis et al. 1977, Papoušek 1979, Harmanec et al. 1980). A summary of the photometric behaviour of 4 Her can be found in Pavlovski et al. (1997).

Available observations now cover a time interval of more than 75 years. An analysis of photographic spectra from two shell episodes and of a rich collection of electronic spectra of 4 Her enabled us:

– to confirm the binary nature of the star and to derive, for the first time, its reliable orbital elements,
– to find evidence for an interaction in a binary system, and
– to document and describe the presence of a fine structure in some shell lines.

2. Observations and reductions

2.1. Spectroscopy

A rich collection of spectroscopic data at our disposal (RV and spectrophotometric measurements) consist of earlier data sets (P5, P6) and of new spectra obtained at the Ondřejov and Haute Provence (OHP) Observatories. Basic information about the new spectra can be found in Tables 1 and 2 (in electronic form only), together with the results of their measurements.

The new spectroscopic material used consists of the following sets of spectrograms:

– 18 blue-violet spectrograms taken with the W camera in the coudé spectrograph of the 1.93-m telescope at OHP,
– 19 blue-violet spectrograms taken with the GB camera in the coudé spectrograph of the 1.52-m telescope at OHP,
– 61 spectrograms covering the blue-violet region taken with the 700 mm camera in the coudé spectrograph of the 2-m telescope at Ondřejov (33 after the refurbishment of the telescope and the spectrograph in 1987),
– 13 spectrograms covering the red region taken with the coudé spectrograph of the 2-m telescope at Ondřejov,
– 66 Reticon spectra taken with the coudé spectrograph of the 2-m telescope at Ondřejov equipped with an image slicer of the type designed by Gazhur & Bikmaev (1990) and covering the range 6300 – 6700 Å,

Table 3. Seasonal mean V, $B - V$ and $U - B$ values of 4 Her (in mag.) and their rms errors per one observation of unit weight (in mmag., in parentheses) from individual observing stations

Mean epoch	No.	V	$B - V$	$U - B$	HD comp.	Stn.
0738.8	25	5.755(21)	−0.114(20)	−0.345(16)	143418	4
1144.8	56	5.751(12)	−0.101(10)	−0.334(10)	144206	13
1543.1	44	5.752(17)	−0.098(13)	−0.348(10)	144206	1
1929.1	35	5.744(13)	−0.094(13)	−0.354(13)	144206	1
2238.5	29	5.741(29)	–	–	142373	40
2267.8	84	5.761(22)	–	–	142373	41
2269.3	7	5.729(11)	−0.108(21)	−0.338(19)	144206	1
2325.9	18	5.736(06)	–	–	142373	42
2510.6	17	5.736(17)	–	–	142373	42
2541.3	48	5.747(20)	–	–	142373	40
2596.2	72	5.752(10)	–	–	142373	41
2620.5	11	5.761(24)	−0.102(14)	−0.353(10)	144206	1
2960.8	9	5.756(07)	−0.128(07)	−0.353(04)	142373	2
2980.7	50	5.755(17)	−0.108(15)	−0.353(13)	144206	1
3275.4	4	5.730(09)	−0.106(08)	−0.345(06)	144206	1
3311.9	10	5.744(06)	−0.119(08)	−0.360(08)	142373	2
3743.3	5	5.751(05)	−0.108(04)	−0.363(11)	144206	1
3778.3	2	5.730(02)	−0.109(03)	−0.335(10)	142373	2
4071.3	5	5.751(08)	−0.099(11)	−0.365(07)	144206	1
4441.0	17	5.744(10)	−0.090(12)	−0.385(21)	144206	1
4791.0	13	5.631(15)	+)	–	144206	20
4811.7	15	5.743(09)	−0.106(11)	−0.375(10)	144206	1
5123.3	76	5.738(12)	−0.105(09)	−0.372(08)	144206	1
5477.4	16	5.735(11)	−0.105(11)	−0.367(12)	144206	4
5871.0	12	5.739(13)	−0.113(09)	−0.368(08)	144206	1
5915.0	4	5.746(17)	−0.114(21)	−0.368(11)	144206	4
6274.4	7	5.744(09)	−0.118(10)	−0.376(07)	144206	1
8036.0	48	5.734(11)	–	–	–	61
8055.9	6	5.734(06)	−0.105(08)	−0.376(06)	144206	15
8114.3	2	5.745(04)	−0.098(10)	−0.368(01)	144206	1
8369.3	36	5.746(17)	−0.105(07)	−0.377(08)	144206	15
8407.3	50	5.756(30)	–	–	–	61
8750.8	29	5.870(23)	–	–	–	61
8791.1	17	5.879(23)	−0.077(16)	–	144206	20
9023.8	3	5.905(08)	–	–	–	61
9154.6	19	5.911(19)	−0.077(11)	–	144206	20
9527.9	7	5.846(31)	−0.109(28)	–	144206	20
9942.0	7	5.802(22)	−0.103(07)	–	144206	20

+) Only B magnitude observations available, mean B is given under V. Column 'Mean epoch' gives the mean HJD−2440000 of each normal point, column 'No.' contains the number of individual observations forming the mean, column 'HD comp.' specifies the HD number of the comparison star used for the given data set – cf. Table 5. Individual data sources (column 'Stn.') are identified by their numerical codes used in the Ondřejov data archives as follows: 1... Hvar 0.65-m Cassegrain reflector; 2... Brno 0.60-m Cassegrain reflector (Papoušek 1979); 4... Ondřejov 0.65-m Cassegrain reflector; 13... Mt. Kobau 0.4-m reflector; 15... Phoenix-10 0.25-m APT reflector; 20... Toronto 0.4-m reflector; 40... Hickox 0.25-m Cassegrain reflector; 41... East Point 0.20-m reflector; 42... Dyer 0.60-m Cassegrain reflector; 61... Hipparcos Catalogue Annex V magnitudes (Perryman et al. 1997): a zero-point correction of +0$.^m$04 had to be added to them.

– 23 CCD spectra taken with the Aurélie spectrograph of the 1.52-m telescope at OHP; 13 spectra cover about 200 Å near Hα; 10 other were centred on 4500 Å.

Table 1 (in electronic form only) summarizes the measurements carried out in the red spectra. With the exception of the Si II 6347 Å line, all other values refer to Hα (RV, the central intensity of shell absorption I_c, intensities of the violet V and red R emission peaks). The three Ondřejov spectrograms Nos. 4720, 4808 and 5136 were taken when the emission was very faint or absent. These spectra were included in order to better describe

the evolution of the envelope discussed in Sect. 3. The tabulated values for V and R are the central intensities measured at the positions corresponding to the maximum of emission peaks during the shell phase. The reduction and measurement of the spectra, both photographic (all plates were scanned with the 5-channel microphotometer of the Ondřejov Observatory) and electronic (for HJD larger than 2448800) were carried out with the help of a Pascal program SPEFO written by the late Dr.J.Horn (see Horn et al. 1992, 1994, 1996 and Škoda 1996 for details). The final correction of the RV zero point of the electronic spectra obtained in the red spectral region was carried out through the measurements of selected telluric lines (see Horn et al. 1996 for details). This way, we can consider the red Reticon and Aurélie spectra as having the same RV zero point.

In Table 2 (in electronic form only) a list of the spectra and RV measurements for the violet-blue region is given. Several spectra in Tables 1 and 2 were already used by P3, P5 and P6. Here we only tabulate the new RV measurements.

Whenever appropriate, the individual RVs were assigned weights according to the formula

$$w = 8 \, Q \, N \, D^{-1}, \tag{1}$$

where D denotes the dispersion (in Å mm^{-1}), N the number of lines measured and Q was set equal to 1 for photographic, and 4 for the electronic spectra. This weighting ensured homogeneity of the new data sets with those of P5 (see Horn et al. 1996 for justification).

2.2. Photometry

We compiled and homogenized UBV data from a number of different sources. Altogether, these observations cover the period from 1970 to 1996. Basic information about all data files for 4 Her and the check stars used can be found in Tables 3 and 4. The rms errors per 1 observation of unit weight are given to characterize the scatter of individual data sets and/or variability within each season. Individual stations are identified by their numerical codes routinely used in the Ondřejov data archives. Three different comparison stars were used but all three were systematically observed at the Hvar Observatory and their accurate mean all-sky UBV magnitudes were derived by Harmanec et al. (1994). For convenience, the comparison-star data are summarized in Table 5.

Observations from Hvar and Ondřejov were reduced to the standard UBV system via non-linear transformation equations (program HEC22 rel.12; see Harmanec et al. 1994 and Pavlovski et al. 1997 for the details on the observations and reductions). Individual observations have been published by Harmanec et al. (1997).

Observations from Mt. Kobau were obtained and reduced to the standard DAO photometric system by Hill et al. (1976) but never published in detail. Standard UBV magnitudes of 4 Her were derived from the Mt.Kobau observations (see Appendix of Hill et al. 1997).

Brno data were published by Papoušek (1979). Using a bilinear transformation to the published all-sky UBV values for several comparison and check stars, we first transformed these data to bring the magnitude differences between 4 Her and χ Her closer to the standard system. Then, we added to them the Hvar all-sky values for χ Her. Data from the remaining stations (Landis et al. 1977, Percy et al. 1988, Percy & Attard 1992) were reduced to the standard UBV system by their authors. In all cases, however, the originally derived magnitude differences between 4 Her and the comparison star were added to the accurate all-sky mean UBV values of Table 5. The level of internal accuracy of individual data sets can in some cases be judged from the rms errors per one observation of unit weight for the check stars – see Table 5. Unfortunately, the group of 4 Her was redefined several times during the Be campaign and we do not have a more homogeneous set of check stars at our disposal.

We also present (in Table 6) an overview of earlier *all-sky* UBV observations and also our reconstruction of the V magnitude of the star based on visual magnitude differences between 4 Her and 6 Her added to the Hvar V magnitude of 6 Her. These were compiled by JRP from several old sources. Note that thanks to the fact that 6 Her has very similar colours to 4 Her, these estimates of the V magnitude of 4 Her should be quite close to the Johnson V magnitude, within the limits of the accuracy of the old data, of course.

3. Long-term variability

The long-term phase changes from almost normal B to Be and Be-shell, and conversely, have been systematically monitored in only very few Be stars. Different quantities were used to describe the spectral variability of particular stars. The episode of activity of 4 Her is characterized by a gradual development of emission in Hα and by appearance of the metallic shell lines.

For a long time, no convincing evidence of light variability of 4 Her was presented, although the scatter of individual observations was somewhat larger than expected for a constant star (cf., e.g., Heard 1940, Landis et al. 1977, Harmanec et al. 1980, Schuster & Alvarez 1983, or Percy et al. 1988). The first clear evidence of secular light changes has been presented by Percy & Attard (1992), Pavlovski et al. (1997), and by Perryman et al. (1997).

3.1. Correlated Hα emission, light and colour changes

4 Her has a very long record of the behaviour of the Hα line. In Fig. 1 we present the estimate of Hα emission strength of 4 Her vs. time.

The same representation as that by Hubert (1971) was used (Hα in emission – 1, Hα in absorption – 0) to allow a direct comparison with his results. Recently the star has entered the third emission-line episode detected since the 1920's. The first episode lasted longer than 5 and shorter than 20 years while the second one lasted about 20 years. The two periods of normal B spectrum are well documented, but their lengths are very different: 13 to 15 years vs. 3 to 5 years.

An interesting, though not simple correlation of the light and colour changes with the dispersal of the old, and formation of a

Table 4. Journal of UBV observations of the check stars used. Julian dates of the first and the last observation, number of observations and the mean *differential UBV* magnitudes (in mag.) with their rms errors per one observation of unit weight (in mmag, in parentheses) are given for each data set

Stn.	Epoch (JD−2400000)	No.	V	B	U	$B-V$	$U-B$	HD comp.
	ϕ Her							
1	41530.4–45196.4	211	4.252(14)	4.189(16)	3.939(20)	−0.064	−0.250	144206
	χ Her							
1	42994.3–48114.4	164	4.606(13)	5.180(14)	5.178(18)	0.575	−0.002	144206
4	45441.5–45441.6	10	4.613(12)	5.185(18)	5.193(14)	0.572	0.008	144206
	50 Boo							
1	45912.4–45913.4	7	5.388(12)	5.305(17)	5.137(17)	−0.083	−0.167	144206
1	46266.4–48116.4	16	5.399(11)	5.333(20)	5.153(14)	−0.066	−0.180	138341
4	45461.5–45936.4	14	5.402(13)	5.337(14)	5.152(16)	−0.066	−0.185	138341
15	48039.7–48432.7	170	5.396(08)	5.332(08)	5.163(06)	−0.064	−0.169	138341
20	48761.7–49951.6	46	5.391(21)	5.325(28)	–	−0.067	–	138341
	HR 5760							
1	45912.4–45913.4	8	6.466(08)	6.643(19)	6.784(11)	0.176	0.141	144206
20	46223.6–46294.6	21	6.476(07)	6.665(09)	–	0.188	–	136849
	HD 141930							
1	45117.4–45155.4	36	7.721(11)	7.813(09)	7.917(16)	0.093	0.104	144206
	HD 143418							
1	45117.4–48114.4	71	7.444(14)	7.603(16)	7.720(20)	0.159	0.118	144206
4	45461.5–45912.4	12	7.437(15)	7.603(11)	7.726(16)	0.166	0.123	144206
15	48044.7–48440.7	41	7.445(09)	7.614(09)	7.714(10)	0.170	0.099	144206

Column 'HD comp.' specifies the HD number of the comparison star used for the given data set – cf. Table 5. Individual data sources (column 'Stn.') are identified by their numerical codes used in the Ondřejov data archives as follows: 1... Hvar 0.65-m Cassegrain reflector; 2... Brno 0.60-m Cassegrain reflector (Papoušek 1979); 4... Ondřejov 0.65-m Cassegrain reflector; 13... Mt. Kobau 0.4-m reflector; 15... Phoenix-10 0.25-m APT reflector; 20... Toronto 0.4-m reflector; 40... Hickox 0.25-m Cassegrain reflector; 41... East Point 0.20-m reflector; 42... Dyer 0.60-m Cassegrain reflector;
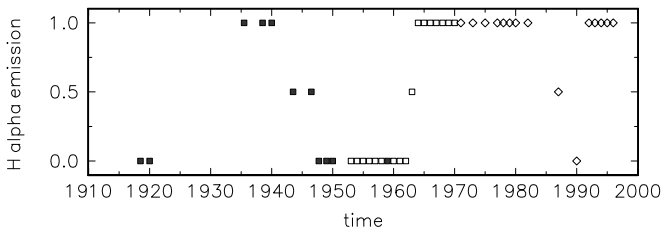

Fig. 1. Schematic representation of Hα emission versus time. Full and empty boxes (Hubert, 1971), diamonds this paper

Table 5. Comparison and check stars used. Improved mean *all-sky UBV* magnitudes, derived by Harmanec et al. (1994), which were invariably used here, are given

Star	HD	V	$B-V$	$U-B$
υ 6 Her	144206	$4\overset{m}{.}741$	$-0\overset{m}{.}097$	$-0\overset{m}{.}325$
ν 11 Her	145389	$4\overset{m}{.}255$	$-0\overset{m}{.}064$	$-0\overset{m}{.}250$
ξ 1 Her	142373	$4\overset{m}{.}607$	$0\overset{m}{.}576$	$-0\overset{m}{.}004$
50 Boo	136849	$5\overset{m}{.}399$	$-0\overset{m}{.}068$	$-0\overset{m}{.}186$
HR 5760	138341	$6\overset{m}{.}473$	$0\overset{m}{.}193$	$0\overset{m}{.}127$
HD 143418	143418	$7\overset{m}{.}444$	$0\overset{m}{.}160$	$0\overset{m}{.}115$
HD 141930	141930	$7\overset{m}{.}721$	$0\overset{m}{.}092$	$0\overset{m}{.}103$

new emission-line envelope is documented by Fig. 2. The upper panel of Fig. 2 shows the time variability of the Hα emission, characterized by the mean peak intensity (V + R)/2 averaged over 100-day intervals. The data with (V + R)/2 < 1 represent the phase of a (nearly) normal B type spectrum. To make the low-amplitude secular light and colour variability of the star easier to follow, the three bottom panels of Fig. 2 show the seasonal mean V, $B-V$ and $U-B$ values from Table 3 (averaged separately for each data set). It is seen that the gradual disappearance of the Hα emission which was continuing since about JD 2440000 until JD 2448000 was accompanied by only a very mild increase of the brightness of the star and by a mild blueing of $U-B$. A much faster re-appearance of the Hα emission

started at about JD 2448300. It was accompanied by a steep decline in brightness and by reddening of the star. Note, however, that the minimum brightness was attained at about JD 2449100 and that the continuing strengthening of the Hα emission was since then followed by another rapid *increase* of the luminosity of the object in the optical region. 4 Her is, therefore, another example of a long-term Be variable for which non-emission phases coincide with phases of maximum brightness and the bluest $B-V$ and $U-B$ (cf. Harmanec 1983).

Table 6. An overview of earlier all-sky UBV photometry of 4 Her

Source	Epoch	V	$B-V$	$U-B$
HAR1908	1796–1799	$5\overset{m}{.}76$	–	–
HAR1884	1880–1882	$5\overset{m}{.}76 \pm 0\overset{m}{.}11$	–	–
HAR1908	1883?	$6\overset{m}{.}06$	–	–
POT	1886–1905	$5\overset{m}{.}80 \pm 0\overset{m}{.}05$	–	–
HAR1899	1892–1894	$5\overset{m}{.}67 \pm 0\overset{m}{.}16$	–	–
HAR1908	1892–1894	$5\overset{m}{.}74$	–	–
C63	1960–1961?	–	$-0\overset{m}{.}12$	$-0\overset{m}{.}42$
LO64	1956–1963	$5\overset{m}{.}75$	$-0\overset{m}{.}11$	–
C73	1965–1973	$5\overset{m}{.}80$	–	–

Sources: HAR1884 – Harvard visual photometry, Pickering (1884), HAR1899 – Pickering (1899), HAR1908 – Pickering (1908): quotes data from older catalogues by Herschel [data from 1796-99], Oxford [about 1883] and Baily [1892-94], POT – Potsdam catalogue of visual magnitudes (Müller & Kempf 1907), C63 – Crawford (1963), LO64 –Ljunggren & Oja (1964), C73 – Crawford et al. (1973). *Notes:* For all old sources of visual magnitude, the differences between 4 Her and 6 Her were added to the Hvar V magnitude of 6 Her. All more recent determinations come directly from the respective all-sky photometries.

Note also that earlier all-sky UBV observations, collected in Table 6, obviously fall within the same range as the data presented here.

Continuing observations of the present emission phase can bring new information about the behaviour of the envelopes and/or disks around early type stars in general.

3.2. Shell spectrum

The shell spectrum of 4 Her is visible in hydrogen lines up to H11, in metallic lines (Fe II, Ti II), and in Ca II, Na I and Si II lines. As noted by Hubert (1971) the shell lines of 4 Her are not typical for a shell star. He found that they were rather broad, corresponding to $v \sin i = 220\,\mathrm{km\,s^{-1}}$. According to Hubert's description, the shell lines of Na I, Si II and Ca II were visible in the spectrum of 4 Her nearly ten years before the onset of the Hα emission episode. However, an inspection of the plates he used showed that a sharp component of the Ca II K line had always been present, becoming much stronger during the Hα emission episode. In Fig. 3 we show the time variation of the equivalent width and central intensity of the Ca II K line measured in the photographic spectra. We note that the initial increase of the strength of the Ca II K line correlates very well with the light decrease at the beginning of the new emission-line phase. Moreover, the Ca II K line develops broad wings during the shell formation (see Fig. 4) – similarly as 88 Her (Hirata 1978, Doazan et al. 1982) or Pleione (Hirata & Kogure 1976). At maximum strength (the bottom profile in Fig. 4) the Ca II K profile can be *formally* characterized by the following parameters: $T_{\mathrm{eff}} \sim 9500\mathrm{K}$, $\log g \sim 3.0$, $v \sin i \sim 200\,\mathrm{km\,s^{-1}}$.

The metallic shell spectrum develops very quickly in the early stages of the envelope formation to a certain strength which remains more or less constant during the gradual increase of the Hα emission. This is documented in Fig. 5 where the metal-
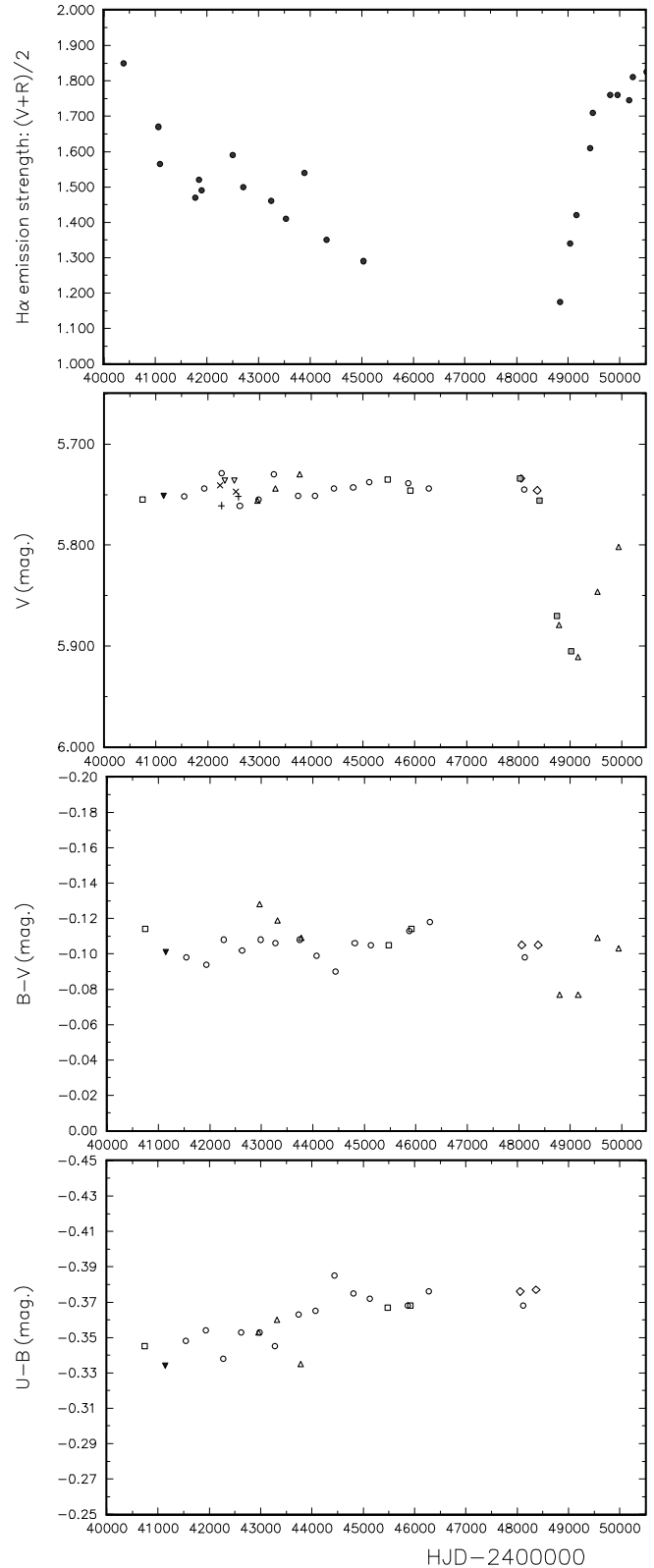

Fig. 2. Long-term Hα emission strength, light and colour variations of 4 Her. The following symbols are used to distinguish the seasonal normals from individual observing stations: circle: Hvar, square: Ondřejov, triangle up: Brno, filled triangle up: Toronto, triangle down: Dyer, filled triangle down: Mt. Kobau, diamond: APT Phoenix, cross: Hickox, plus: East Point, full square: Hipparcos
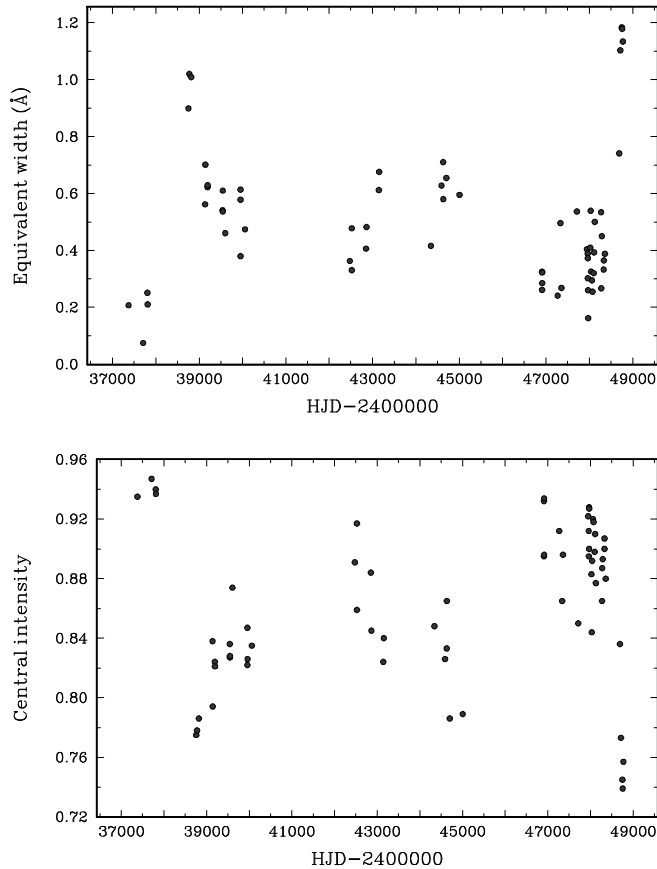
Fig. 3. Time variation of the equivalent width and central intensity of the Ca II K line of 4 Her
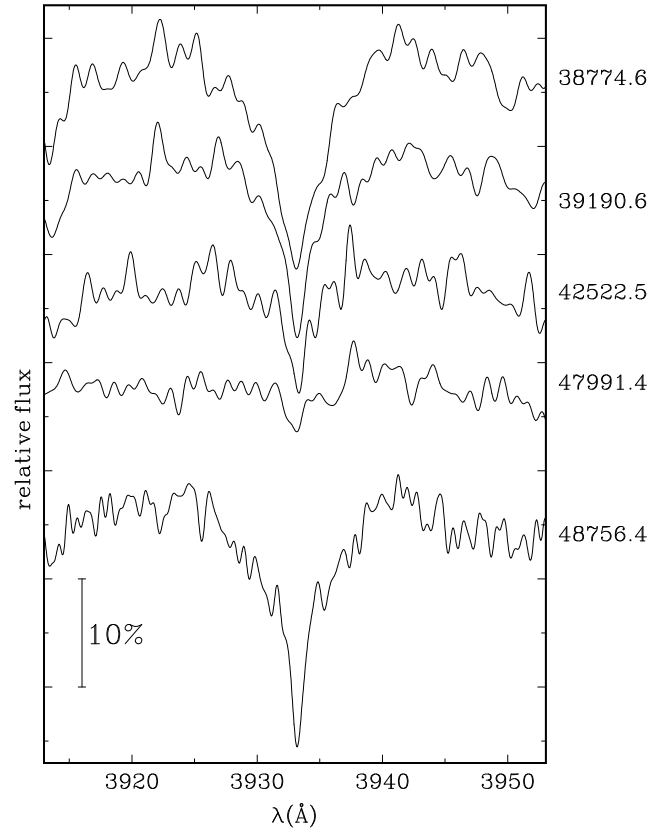

Fig. 4. Selected Ca II K line profiles. Note the broad wings of the profile which develop during the early stages of the formation of a new shell. The profiles are identified by HJD−2400000 on their right side

lic shell lines in the region around 4500 Å are compared to nearly simultaneous spectra of Hβ or Hα for two different shell episodes.

3.3. Central quasi-emission bumps

One of the most interesting features visible in the spectrum of 4 Her is the apparent doubling of some shell lines. It was first reported by Koubský et al. (1993) and interpreted as one of the signatures of the beginning of a new shell episode. The feature had been stable over four months. This was why the structures were tentatively called central quasi-emission bumps (CQEB). As this "doubling" occurs on the level of a few percent of the continuum intensity only, high-S/N spectral observations are essential for monitoring. The left bottom panel in Fig. 5 documents the time development of the phenomenon during the most recent shell episode. It is seen that the CQEB are strongest around the minimum brightness of the object. They are then becoming fainter as the Hα emission continues to strengthen (see Fig. 5).

The nature of CQEBs remains unclear. In a sense, they resemble Zeeman-splitted lines in the presence of a magnetic field but such an explanation can clearly be ruled out since also lines insensitive to Zeeman splitting exhibit CQEB.

4. Variations on other time scales

The scatter of individual observations of 4 Her is generally higher than what one would expect for a constant star. Our data do not show compelling evidence of variations on time scales from days to weeks.

UBV photometry available to us is not very suitable to a search for rapid changes since only a few longer series of observations during the night were secured. The plots of these night series show systematic trends in some cases and constant light in others. However, we note that in only two cases (HJD 2441536 and 24445441) variations can be suspected for observations obtained relative to the most frequently used comparison 6 Her. Even in these cases, however, a simultaneous plot of the check star magnitude does not render the case of real rapid changes of 4 Her particularly convincing.

5. Phase-locked variations with the 46-day period

5.1. Improved value of the period

P3 and P5 found periodic radial velocity changes in 4 Her with a 46-day period. P6 showed that also some spectrophotometric quantities display clear phase diagrams when folded with this period. The data string now available is much longer and we thus
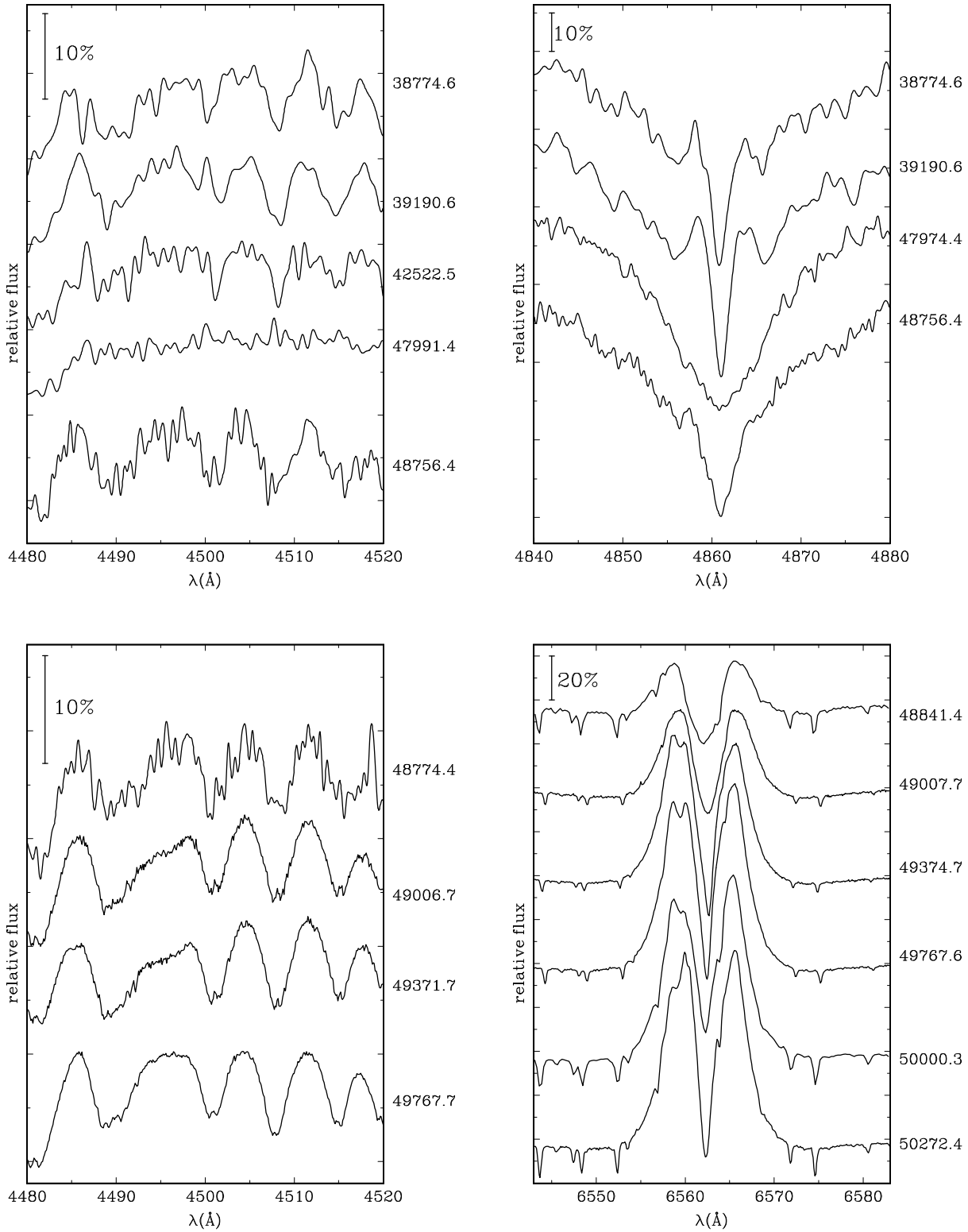
Fig. 5. A comparison of nearly simultaneous Hβ or Hα and metallic-line profiles in the region around 4500 Å from two different shell phases. The profiles are identified by HJD−2400000 on their right side

tried to check the stability of the derived period and to improve its value. Since all available RVs for historical data are based on the H I *shell* lines, a complete set of H I shell RVs was used to the determination of an improved value of the period. We, therefore, combined all RVs from P5 with the new H I shell RVs obtained here (excluding Hα RVs). Though we used the code for the solution of binary elements FOTEL (Hadrava 1990), we primarily tried to describe the periodic behaviour of the RVs. We leave the discussion of the binary system to Sect. 6. Allowing for six different γ-velocities (DAO prism, DAO grating, DDO prism, DDO grating, OHP [W camera] and Ondřejov), we calculated a formal orbital solution for these data with the period as one of the elements to be solved, and obtained

$$
\begin{aligned}
T_{\mathrm{max.RV}} = &\ (\text{HJD } 2441473.07 \pm 0.98) \\
&+ (46^{\mathrm{d}}1921 \pm 0^{\mathrm{d}}0023) \times E,
\end{aligned}
\tag{2}
$$

the rms of 1 observation of unit weight being $3.92\,\mathrm{km\,s^{-1}}$. This result has not changed significantly when we used one common γ-velocity in the solution. We also calculated free solutions for several other data sets, with the following results:

$46^{\mathrm{d}}192 \pm 0^{\mathrm{d}}004$ for the Hα shell,

$46^{\mathrm{d}}183 \pm 0^{\mathrm{d}}012$ for the wings of Hα emission

$46^{\mathrm{d}}187 \pm 0^{\mathrm{d}}011$ for the broad H I, and

$46^{\mathrm{d}}193 \pm 0^{\mathrm{d}}011$ for the metallic shell lines.

All these values agree with the period of ephemeris (2) within the limits of their errors.

We also carried out a test on the possible secular change of the 46-d period splitting the data into two parts in time. We found a period decrease which appears formally significant within the error limits, calculated values of ω remaining almost the same in both subsets. Solution for all H I shell RVs in which we allowed for calculation of a period derivative (estimated from the two subsets of the RV data) led to the following quadratic ephemeris:

$$
\begin{aligned}
T_{\mathrm{max.RV}} = &\ (\text{HJD } 2441473.47 \pm 0.78) \\
&+ (46^{\mathrm{d}}1809 \pm 0^{\mathrm{d}}0053) \times E \\
&+ (5.2 \pm 2.0)10^{-6} \times E^2,
\end{aligned}
$$

the rms of 1 observation of unit weight being $3.85\,\mathrm{km\,s^{-1}}$. This would imply a very large period decrease of 71 s per year. We are currently unable to exclude the presence of such a period change but we note that the effect is mainly dictated by the data from prismatic spectrograms. Only continuing RV observations will allow to exclude with certainty this suspected period change.

For the moment, we feel justified to adopt the linear ephemeris (2), based on all H I shell RVs, throughout the rest of this study.

5.2. Phase-locked variations of circumstellar lines

In Figs. 6, 7, 8, and 9 (bottom panel) we present phase plots of several quantities measured in the Hα profiles: central intensity, ratio of emission peaks, RV of the absorption core and RV of Hα
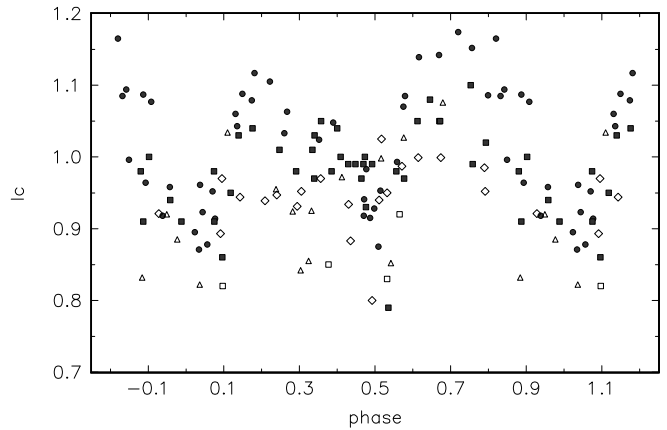

Fig. 6. Phase plots of the central intensity of Hα. The following symbols are used to distinguish data from various epochs: Full boxes: observations before 43500 (JD−240000), open boxes: 43500 – 45000, diamonds: before 49370, triangles: 49370 – 49800, full circles: after 49800. All spectra after 45000 are from electronic detectors.

emission wings, respectively. For spectrograms obtained before JD 2442200 values from P6 were adopted and are shown in the above mentioned figures, but not in Table 1. All four figures include data from *two separate* Be/shell episodes two decades apart. The observations from both episodes can be folded with the same period and phase. The phase dependence of I_c is better defined when the emission in the Hα line is well developed (solid symbols). This is not so obvious for V/R.

RV of the Hα absorption core attains the maximum near the elongation with the Be star receding, i.e. near phase 0.0. A secondary RV maximum occurs between phases 0.3 and 0.5. At the same time, the core is deepest near phases 0 and 0.5 (near conjunctions) and shallowest at phases 0.2 and 0.72. The V/R variation of the double Hα emission attains a sharp maximum near phase 0.85 and a secondary one at about 0.39. The formal orbital solution for the RVs of Hα absorption core leads to the eccentricity $e \sim 0.5$ which is mainly due to the fact that the RV of Hα absorption is much more positive than the velocity of the centre of Hα emission near phase 0.0. This difference is also seen if one compares the upper panel in Fig. 8 and the bottom panel in Fig. 9. Fig. 7 clearly shows that also the phase curve of the V/R ratio of Hα is highly non-sinusoidal. Moreover, it attains the principal maximum at phase $0^{\mathrm{p}}9$ with respect to the H I shell RV maximum (phase 0.0 of ephemeris (2)).

P5 measured also RVs of some metallic shell lines. They remarked that these lines were barely measurable and a few metallic velocities were in fair agreement with the velocities of the hydrogen lines. The results of the measurements on electronic spectra are given in Table 1 (Si II 6347Å from Reticon), column ' Si II', and in Table 2 (Fe II lines from Aurélie), column 'M shell'. A phase diagram showing the metallic RVs from both the DDO photographic and new electronic spectra is in the bottom panel of Fig. 8. It is seen that the RV curve of the metallic lines is nearly circular (eccentricity ~ 0.1 and resembles more the RV curve of the broad H I lines (middle panel in Fig. 9) or
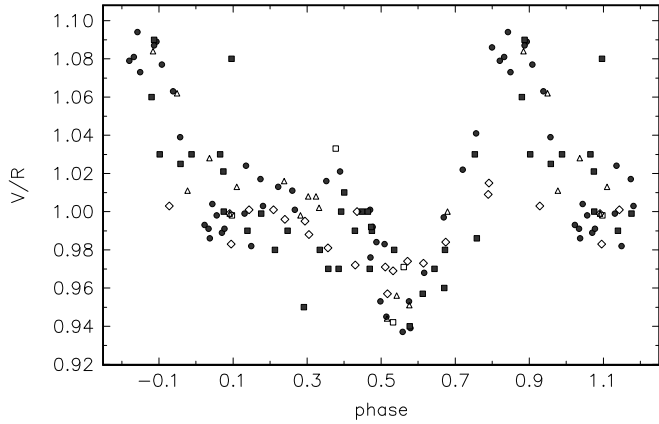
Fig. 7. Phase plots of the V/R ratio of the Hα emission. The same symbols as in Fig. 6 are used

the wings of Hα emission (bottom panel in the same figure) than that of the Hα absorption core.

A fascinating absorption feature was discovered in the violet peak of the Hα emission line. It is detectable during most of the orbital phases. It moves from blue to red across the emission peak until it reaches a RV of about -90 km s^{-1} and then reappears again with a RV of -190 km s^{-1}. It can be seen in four of the Hα spectra shown in Fig. 5. Its RV is also tabulated in column 'ABSF' of Table 1. It is observable only when the Hα emission strength exceeds ~ 1.5 of the continuum level. It is somewhat reminiscent of a similar feature reported recently by Pogodin (1997) for HD 50138 which, however, is not known to be a periodic RV variable. In the case of 4 Her, this phenomenon – which has so far been monitored for more than 1300 days – repeats strictly with the $46\overset{d}{.}192$ clock (see Fig. 10).

5.3. Orbital light variations

To check on the possible presence of low-amplitude light variations related to the binary orbit, we used 1-d normal points prewhitened for the long-term light variations by means of Vondrák's (1969, 1977) smoothing technique. Our data safely exclude the presence of deep binary eclipses. The results are similar to conclusions by Landis et al. (1977).

6. The binary system of 4 Her

The first preliminary determination of the orbital elements of the star based on photospheric lines was presented by Koubský et al. (1994). The most obvious interpretation of the observed variations described in the previous section is to take them as a consequence of orbital motion in a binary system. The different sets show different semiamplitude of RV variation K and/or different shape of the RV curve (expressed as non-zero eccentricity). One has to select a set which would describe the motion of the star with minimal influence of the atmosphere and/or circumstellar matter. In principle, the orbital elements of 4 Her can be based on measurements of
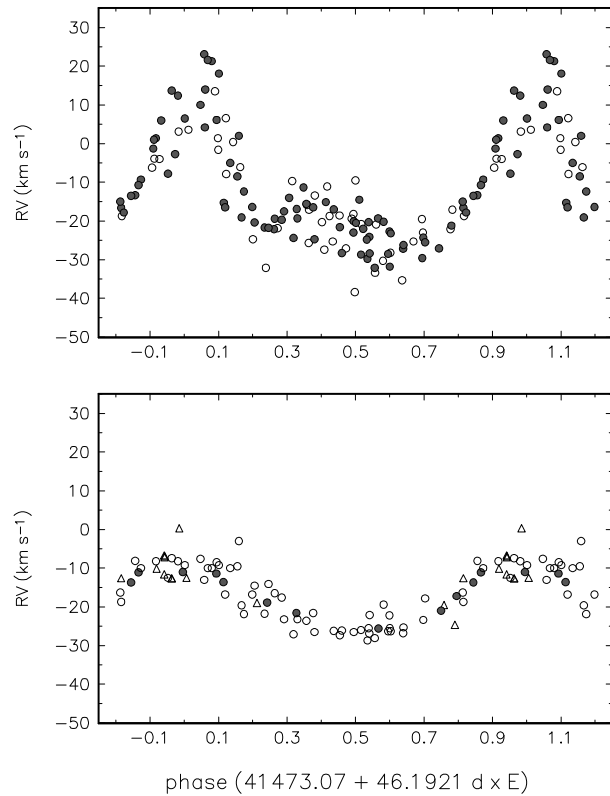

Fig. 8. Phase plots of the RV of the shell lines of 4 Her. *Upper panel:* Hα absorption core: open and filled circles denote RVs from the photographic and electronic spectra, respectively. *Lower panel:* metallic lines: triangles... photographic DDO spectra, open circles... red electronic spectra, filled circles... blue electronic spectra

- photospheric components of hydrogen lines,
- hydrogen lines during periods of normal B absorption spectrum,
- wings of the double Hα emission.

RVs of broad hydrogen lines (Table 2, column 'H stel') and of the centre of the double Hα emission (Table 1, column 'emission') are plotted vs. phase for our adopted ephemeris in the two panels of Fig. 9. The two curves differ: while they are both roughly sinusoidal, the RV curve of the broad H I absorption lines is slightly blue-shifted and has a large range of about -15 to -30 km s^{-1}, compared to -10 to -20 km s^{-1} for the Hα emission. This is confirmed by the circular orbital solutions – see Table 7, columns 'H stel' (broad hydrogen lines) and 'Hα emission' (Hα emission wings). Note, however, that for both these solutions, the semiamplitudes of RV variations are much lower than those derived from the Balmer shell lines ($10 - 16$ km s^{-1}, P3, P5, P6).

A reasonably low scatter around the mean curve seen in the bottom panel of Fig. 9, especially for RVs from the electronic spectra, suggests not only that the centre of Hα emission can be measured quite reliably but also that at least those parts of the circumstellar envelope of 4 Her, in which the steep wings of the Hα emission originate, are reasonably symmetric and secularly

Table 7. Circular and elliptical orbital elements of 4 Her based on RVs from broad H I lines and from Hα emission wings. The orbital period $46\overset{d}{.}1921$ was kept fixed in all solutions. Various systemic velocities are distinguished in the individual solutions as follows: *H stel*: 1... Ondřejov photographic, 2... OHP W, 3... OHP GB; *Hα emission* : 1... Ondřejov photographic, 2... electronic spectra;

Element	H stel		Hα emission	
K (km s^{-1})	8.0 ± 0.9	8.2 ± 1.5	4.8 ± 0.7	4.8 ± 3.8
$T_{\mathrm{max.RV}}$	41473.7 ± 0.6	41472.2 ± 4.2	41473.6 ± 0.6	41472.6 ± 8.5
$T_{\mathrm{periastr.}}$	–	41454.9 ± 4.2	–	41453.2 ± 8.5
γ_1 (km s^{-1})	-20.5 ± 0.5	-20.4 ± 0.5	-19.4 ± 0.8	-19.3 ± 0.8
γ_2 (km s^{-1})	-15.3 ± 1.5	-14.8 ± 1.5	-17.3 ± 0.3	-17.1 ± 0.3
γ_3 (km s^{-1})	-19.3 ± 0.9	-19.5 ± 0.9	–	–
e	0 fixed	0.175 ± 0.084	0 fixed	0.124 ± 0.093
ω (deg.)	–	213 ± 34	–	203 ± 66
rms(km s^{-1})	4.53	4.42	2.40	2.37
No. of RVs	97	97	104	104

Fig. 10. Phase plots of the RV variation of the absorption feature in the violet peak of Hα emission line
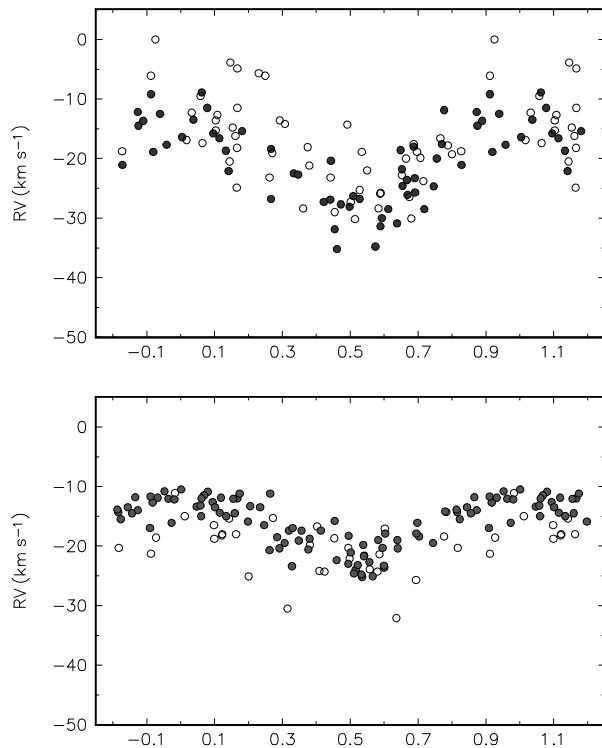
Fig. 9. Phase plots for the adopted ephemeris (2). Upper panel: RVs of the broad hydrogen profiles (full circles: measurements from normal B phase, open circles: shell phase), bottom panel: RV of the Hα emission wings (open circles: photographic plates from the previous Be phase, full circles: electronic spectra from the contemporary Be phase)

stable. The orbital solution 'Hα emission' has lower rms error than the solution 'H stel'. We arrive at the conclusion that in the case of 4 Her RV measurements of the steep wings of the Hα emission provide the best available description of the orbital motion of the Be primary.

To illustrate the range of remaining uncertainties in the current knowledge of the orbital motion of the Be primary of 4 Her, we shall consider both of these solutions in the discussion of the
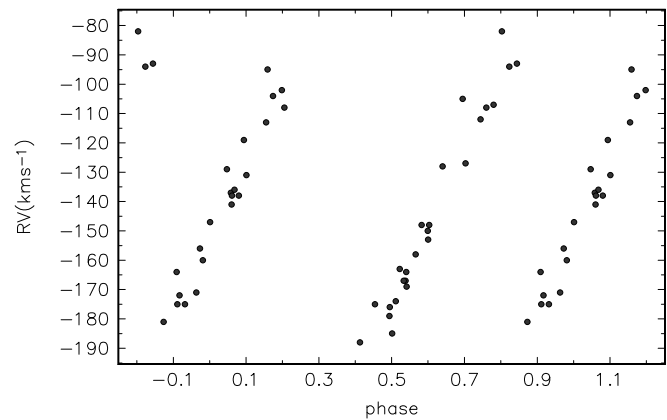
properties of the binary system. Moreover, we also give in Table 7 unconstrained solutions calculated for an eccentric orbit. Both broad H I absorptions and the centre of the Hα emission led to similar orbits with *identical* orientations with respect to us. Therefore, the possibility that the true binary orbit is slightly eccentric must also be kept in mind, though the eccentricity is only barely significant.

6.1. Be primary

We analyzed the spectra of 4 Her with the help of model atmospheres in order to obtain information about the primary. Since 4 Her is a complicated object, accurate model atmosphere analysis based on the best up-to-date NLTE model atmospheres (e.g. Hubeny & Lanz 1995, Dreizler & Werner 1993) could not not be applied until the geometry of the system is known. We, therefore, find it adequate as the first-order approximation to use simpler model atmospheres, based on the assumptions of plane parallel geometry, hydrostatic and radiative equilibrium, and local thermodynamic equilibrium (LTE). Consequently, we used a grid of LTE line blanketed solar-composition model atmospheres of Kurucz (1993).
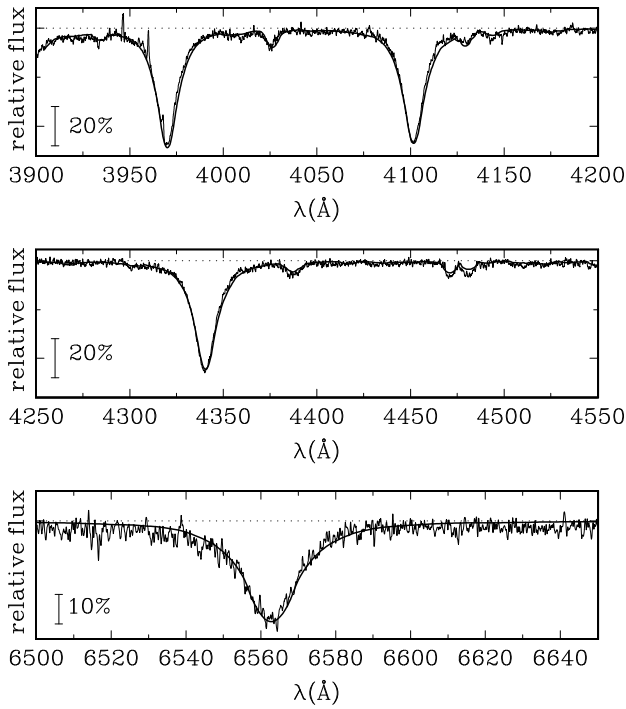
Fig. 11. Comparison of photographic spectra obtained during the phase without a shell with theoretical spectra for a LTE line blanketed Kurucz (1993) model atmosphere with $T_{\mathrm{eff}} = 12500\,\mathrm{K}$, $\log g = 4.0$, and $v \sin i = 300\,\mathrm{km\,s^{-1}}$.

6.1.1. Primary star during the phase of normal B spectrum

First we made a fit to the spectra for the time interval when no shell lines were present. Regrettably, we only have photographic spectra from this phase. Using the above mentioned grid of LTE model atmospheres, the best match (see Fig. 11) is achieved for the following parameters: $T_{\mathrm{eff}} = 12500\,\mathrm{K}$, $\log g = 4.0$, $v \sin i = 300\,\mathrm{km\,s^{-1}}$. The parallax of 4 Her measured by Hipparcos is $\pi = 0\overset{\prime\prime}{.}00667$ (Perryman et al. 1997) which gives the distance to the star $d = 150\,\mathrm{pc}$. Assuming negligible interstellar absorption, $T_{\mathrm{eff}} = 12500\,\mathrm{K}$, $V = 5\overset{\mathrm{m}}{.}745$ (from non-emission phases), and B.C. $= -0\overset{\mathrm{m}}{.}84$ (interpolated from Popper 1980), one arrives at $M_{\mathrm{bol.}} = -0\overset{\mathrm{m}}{.}97$ and $R_1 = 2.9 R_\odot$. According to Popper's (1980) T_{eff} calibration, this corresponds well to a star slightly cooler than B7. According to Harmanec's (1988) calibration, mass and radius of a main sequence star with $T_{\mathrm{eff}} = 12500\,\mathrm{K}$ are $M_1 = 3.2 M_\odot$, $R_1 = 2.6 R_\odot$.

These estimates are remarkably consistent. It is also useful to estimate the possible range of the critical (break-up) rotational velocity of the primary. To a very good approximation, the equatorial radius (R_{e}) of a star rotating at critical speed is $1.5\times$ larger than its polar radius (R_{p}). The polar radius is comparable to the radius of a non-rotating star. Therefore, for mass and radius from Harmanec (1988), the break up velocity must be calculated for $1.5\times$ the radius and amounts to $395\,\mathrm{km\,s^{-1}}$. On the other hand, the radius estimated from the visual magnitude and distance for a star rotating at break-up and not observed just pole-on will be an effective radius which relates to polar
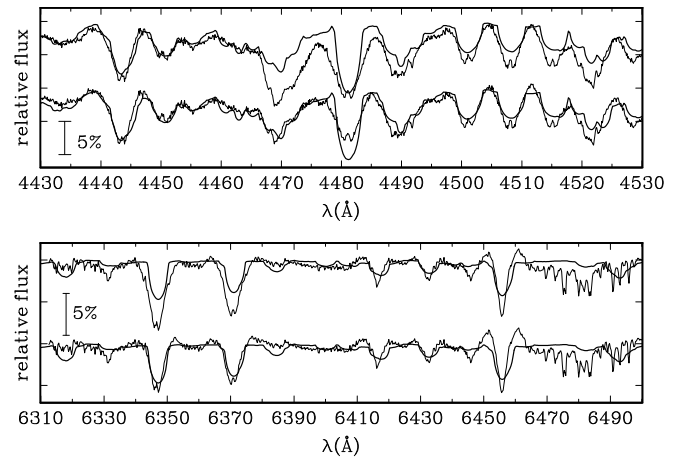

Fig. 12. Comparison of electronic spectra obtained during the shell phase with theoretical spectra for a LTE line blanketed Kurucz (1993) model atmosphere with $T_{\mathrm{eff}} = 8500\,\mathrm{K}$, $\log g = 2.0$, and $v \sin i = 150\,\mathrm{km\,s^{-1}}$ (upper plots on both panels). Lower plots on both panels compare the stellar spectrum with a difference spectrum obtained by subtracting the 0.86 multiple of the original non-shell synthetic spectrum ($T_{\mathrm{eff}} = 12500\,\mathrm{K}$, $\log g = 4.0$, and $v \sin i = 300\,\mathrm{km\,s^{-1}}$) from the synthetic spectrum for $T_{\mathrm{eff}} = 8500\,\mathrm{K}$, $\log g = 2.0$, and $v \sin i = 150\,\mathrm{km\,s^{-1}}$.

and equatorial radii via $1.5 \times R_{\mathrm{p}} \times R_{\mathrm{p}} = R_1^2$. This would imply a break-up speed of $415\,\mathrm{km\,s^{-1}}$. If the equatorial plane of the primary and the orbital plane are identical, these estimates and $v \sin i$ derived here imply that the binary is observed under an inclination higher than $46°$.

6.1.2. Primary star during the shell phase

Recent spectra from the "shell phase" in the blue region around 4470Å can be fitted quite satisfactorily with a plane parallel model of lower temperature, lower gravity, and slower rotation, namely $T_{\mathrm{eff}} = 8500\,\mathrm{K}$, $\log g = 2.0$, and $v \sin i = 150\,\mathrm{km\,s^{-1}}$ (upper spectrum in the upper panel of Fig. 12). This indicates that the atmosphere of the primary extends during the shell phase with lower "effective rotation" and the star *appears* to be cooler. However, there is an obvious difference between a real A3 supergiant (with the above mentioned stellar parameters) and the 4 Her primary, since we know for sure that during the period without shell the observed spectrum of the primary corresponds to a rapidly rotating B7 star. The A3 type spectrum in the region around 4470Å is probably a product of an opaque material (a "shell") orbiting the primary with a rotational velocity that continuously decreases outwards. It may produce a rather unusual temperature and density structure of the "shell" and this can be the reason for the appearance of CQEBs. Such a conjecture should be supported by detailed calculations.

The fact that the primary in the shell phase is not an A3 supergiant is also evident from the fit in the red region, where neither Hα nor Si II lines fit the data. The Hα line is in emission, and the Si II lines 6347 and 6371Å are deeper than predicted by the model (upper spectrum in the bottom panel of Fig. 12).
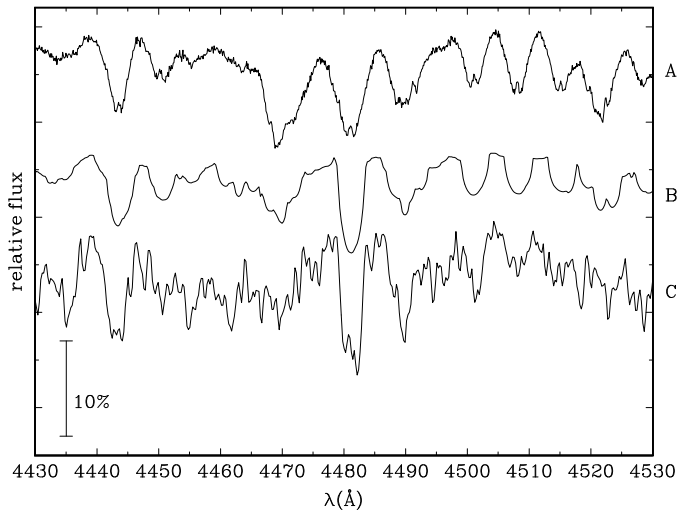
Fig. 13. A Shell spectrum of 4 Her No. a03_202, **B** synthetic spectrum for T_{eff} = 8500K, $\log g$ = 2.0, and $v \sin i$ = 150 km s^{-1}, **C** a sum of **B** with a synthetic spectrum for T_{eff} = 3500K, $\log g$ = 1.5, and $v \sin i$ = 25 km s^{-1} (synchronous rotation).

No matter whether the new envelope is created by mass transfer from the secondary or by outflow from the primary, our observations seem to indicate that a slightly cooler and rotationally flattened pseudophotosphere is formed at the equatorial regions of the star. Let us assume that we observe the object under an inclination different from 90°. Then the newly formed flattened envelope, optically thick in the continuum, will shield the radiation of a part of the B7 photosphere. To make a semi-quantitative test on this model, we used the observed light curve to estimate the loss of continuum radiation from the photosphere of the B7 star during the light minimum of the long-term cycle. It turned out from the V and B light curves that the light was attenuated to about 86 % of its original value in the visual, and to 83 % in the blue part of the spectrum. We, therefore, subtracted the above-derived synthetic spectrum of the primary (12500K), attenuated by these factors, from the observed spectra of 4 Her corresponding to the light minimum, and checked whether the remaining residual shell spectrum can be described by a synthetic spectrum. In Fig. 12 we again compare such residual spectra with a synthetic one for T_{eff} = 8500K, $\log g$ = 2.0, $v \sin i$ = 150 km s^{-1} (lower spectra in both panels). One can see that the agreement is quite satisfactory, even better than for a non-composite spectrum. It is clear that this description is an idealization of the real situation. A real physical model will have to consider smooth temperature variation. Note that our interpretation is similar to, but not identical with the interpretation put forward for the long-term variation of this type by Hirata (1995).

6.2. Mass ratio and the dimensions of the binary system

The two circular-orbit solutions of Table 7 lead to the following values of mass function and projected distance of the compo-

nents: $f(m) = 5.45 \cdot 10^{-4} M_{\odot}$ and $A \sin i = 81.5 R_{\odot}$ for Hα emission, and $f(m) = 2.48 \cdot 10^{-3} M_{\odot}$ and $A \sin i = 82.5 R_{\odot}$ for the broad H I lines. The observed $v \sin i$ together with the estimated break-up rotation speed imply $i > 40°$. This in turn implies that the separation of the binary components must lie between 82 and 84$R_{\odot}$, the mass ratio between 0.06 and 0.16 and, therefore, the mass of the secondary should be between 0.18 and 0.50$M_{\odot}$. Specifically for the solution based on the Hα emission, the binary properties at both extremes of possible inclinations are as follows: for $i = 40°$, the binary mass ratio is 0.091, therefore $M_2 = 0.29 M_{\odot}$ and $A = 82.2 R_{\odot}$. The radii of the corresponding Roche lobes around the primary and secondary are 39.9 and 22.6$R_{\odot}$. For $i = 90°$, $M_2/M_1 = 0.058$, $M_2 = 0.18 M_{\odot}$, $A = 81.5 R_{\odot}$, $R_1^{\text{Roch}} = 39.5 R_{\odot}$ and $R_2^{\text{Roch}} = 22.4 R_{\odot}$.

6.3. Secondary component

P6 argued that 4 Her is an interacting binary system consisting of a Be primary and a cool (later than G) secondary filling its Roche lobe (and remaining undetected in their spectra). The secondary was believed to be losing mass towards the primary via a gas stream that was assumed to be responsible also for the formation and for the temporal variations of circumstellar matter in the system.

While attractive in principle, their hypothesis does not seem tenable any longer. Dougherty et al. (1991) included 4 Her in their near-IR survey of Be stars. The position of 4 Her in the colour diagrams $[H - K]/[J - H]$ and $[J - K]/[K - L]$ in (Dougherty et al. 1994) corresponds to a normal B star without any evidence for a late type companion star. We stress that their technique is quite sensitive since large cool companions to some other Be stars, known from spectroscopy, were detected this way.

As we have demonstrated in the previous subsection, the radius of a Roche-lobe filling secondary is well constrained at about 22.5$R_{\odot}$ for the whole plausible range of orbital inclinations. Let us consider the relative brightnesses of a putative Roche-lobe filling secondary and the Be primary in the visual region for two effective temperatures, 5000 and 3500 K. One obtains $M_{\text{bol2}} = -1^{\text{m}}55$ and $0^{\text{m}}00$, respectively. Applying again Popper's (1980) bolometric corrections, this implies $M_{\text{V2}} = -1^{\text{m}}24$ and $+1^{\text{m}}93$, respectively. This is to be compared to $M_{\text{V1}} = -0^{\text{m}}13$ derived here. Clearly, the Roche-lobe filling secondary with an effective temperature of 5000K is excluded since it would dominate the visual spectrum of the binary.

Using the appropriate brightness ratios, we calculated the sum of synthetic spectra of the Be primary and a 3500K secondary, rotating synchronously with the orbital revolution, i.e. with a projected velocity of 25 km s^{-1}. The results are displayed in Figs. 13 and 14. It is clearly seen that the spectral lines of the secondary should be detectable even in the photographic spectra. Note that this detection would also be facilitated by the orbital RV variations of the secondary for more than ± 30 km s^{-1}. One can, therefore, conclude that a Roche-lobe filling secondary, even as cool as 3500K, can be safely ruled out.
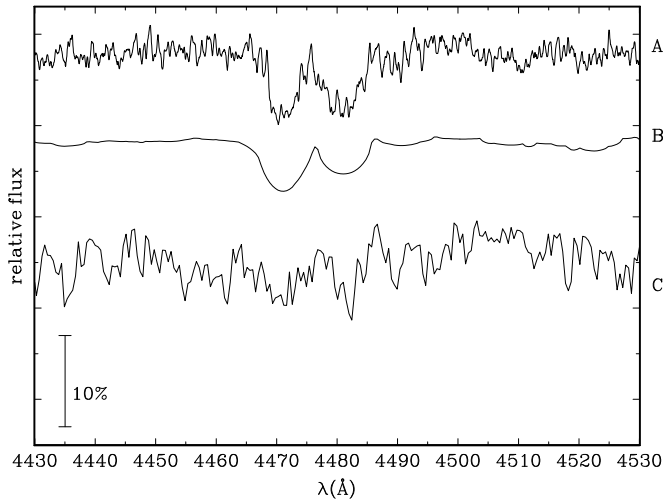
Fig. 14. **A** Non-shell photographic spectrum of 4 Her No. 5122, **B** synthetic spectrum for $T_{\rm eff}$ = 12500K, $\log g$ = 4.0, and $v \sin i$ = 300 km s^{-1}, **C** a sum of **B** with a synthetic spectrum for $T_{\rm eff}$ = 3500K, $\log g$ = 1.5, and $v \sin i$ = 25 km s^{-1} (synchronous rotation).

Judging by the analogy with some other Be binaries (like φ Per, cf. Božić et al. 1995), the secondary could also be a small hot star. Thus, we assumed that the secondary is an sdO star with $T_{\rm eff}$ = 50000K and $\log g$ = 5.5. Since no such model is available in the grid of Kurucz (1993), we calculated a simple LTE hydrogen-helium plane-parallel model atmosphere using the code developed by Kubát (1994, 1996, 1997). Without showing the results in detail we conclude that we are not able to exclude the presence of a sdO or a white-dwarf secondary. High S/N spectra, covering the region of He II 4686 Å line and obtained preferably during the normal B phase would be crucial to check on this possibility.

We also made several unsuccessful attempts to find some spectral lines of the secondary (of any possible type) using the powerful disentangling technique developed by Hadrava (1995). The results were completely negative.

We conclude, therefore, that the secondary star must have a very small radius in comparison to the Be primary.

7. Towards a model of 4 Her

Although the negative results of our attempts to find any *direct* evidence of the secondary component would leave the question of the duplicity of 4 Her open, we can hardly envisage any other mechanism than the duplicity of the object to explain the well-documented phase-locked variations with the 46$^{\rm d}$2 period.

We are left with two most probable possibilities. Either the secondary is a late type star with a small radius ($< 1 R_{\odot}$) which modulates the shape of the emission envelope formed around the primary by its gravity. However, we would run into serious troubles if we would try to explain the complicated observed phase-dependent changes mentioned above.

The other possibility is that the secondary is a hot and rather compact remnant from the previous phase of the mass transfer from the secondary towards the primary and which rapidly shrank to a hot helium star. Horn & Harmanec (1973) found that such a contraction should lead to a rotational instability at the equator and, therefore, to another phase of mass transfer towards the primary, Kříž (1982) and Harmanec (1985) developed the idea of this "post-case-B" mass transfer further. An attractive aspect of this model in relation to 4 Her is that a contracting secondary rotating at break-up speed can lose mass towards the primary even if it is significantly smaller than its Roche lobe.

If there is indeed a gas stream from the secondary towards the primary, it will be deflected by the Coriolis force in the direction of the orbital revolution from the line joining the two stars. A putative hot spot (a region of the impact of the stream into dense parts of the already existing disk) could then be responsible for the principal V/R maximum and its phase shift.

8. Summary

1. Our study reinforces the conclusion of P6 that 4 Her is an interacting binary system, but our results clearly exclude the existence of a Roche-lobe filling secondary. Instead, we suggest that the secondary is a hot and rotationally unstable star. Such a model is capable to explain complicated phase-dependent spectral variations, found by P6 and by us. Note that the phase-locked variations observed during two distinct shell episodes twenty years apart can be folded *with the same period and the same phase*.

2. One of the most exciting results of this study is the discovery of a faint blue-shifted absorption feature with a very unusual but strict phase dependence on the binary orbit. It re-appears exactly at the phases of the V/R maxima, with radial velocities of -190 km s^{-1}. This feature could be traced in the Hα spectra over more than 1300 d. The two occurrences of this absorption do not follow each other after one half of the orbital period. We suggest that it is formed in some region located between the two stars. However, we are currently unable to explain its origin and nature.

3. The pattern of the correlated long-term light and spectral variations of 4 Her was found to be closely similar to that observed also for 88 Her and BU Tau. We have shown that the formation of a new Be envelope can be understood as a process which starts as a flattened, optically thick region around the stellar equator (a pseudophotosphere, cooler than the star itself) which only gradually grows into an extended Be envelope.

References

Božić H., Harmanec P., Horn J. et al., 1995, A&A 304, 235

Crawford D.L., 1963, ApJ 137, 530

Crawford D.L., Barnes J.V., Golson J.C., Hube D.P., 1973, AJ 78, 738

Doazan V., Harmanec P., Koubský P., Krpata J., Žďárský F., 1982, A&A 115, 138 (P7B)

Dougherty S.M., Taylor A.R., Clark T.A., 1991, AJ 102, 1753

Dougherty S.M., Waters L.B.F.M., Burki G. et al., 1994 A&A 290, 609

Dreizler S., Werner K., 1993, A&A 278, 199

Gazhur E.B., Bikmaev I.F., 1990, Astrofizicheskie Izvestija No. 32

Hadrava P., 1990, Contr. Astron. Obs. Skalnaté Pleso 20, 23

Hadrava P., 1995, A&AS 114, 1

Harmanec P., 1983, Hvar Obs.Bull. 7, 55

Harmanec P., 1985, Bull. Astron. Inst. Czechosl. 36, 327

Harmanec P., 1988, Bull. Astron. Inst. Czechosl. 39, 329

Harmanec P., Koubský P., Krpata J., 1973, A&A 22, 337 (P3)

Harmanec P., Koubský P., Krpata J., Žďárský F., 1976, Bull. Astron. Inst. Czechosl. 27, 47 (P6)

Harmanec P., Horn J., Koubský P. 1980, Be Star Newsletter No.. 2, 3

Harmanec P., Horn J., Koubský P. et al., 1980, Bull. Astron. Inst. Czechosl. 31, 144

Harmanec, P., Horn, J., Juza, K., 1994, A&AS 104, 121

Harmanec P., Pavlovski K.,Božić H. et al., 1997, J. Astron. Data, in press

Heard J.F., 1939, J. Roy. Astron. Soc. Canada 33, 384

Heard J.F., 1940, Publ. David Dunlap Obs. 1, 201

Heard J.F., Hurkens R., Harmanec P., Koubský P., Krpata J., 1975, A&A 42, 47 (P5)

Hill G., Hilditch R.W., Pfannenschmidt E.L., 1976, Publ. Dom. Astrophys. Obs. 15, 1

Hill G., Harmanec P., Pavlovski K. et al., 1997, A&A 324, 965

Hirata R., 1978, Inf. Bull. Var. Stars No. 1496

Hirata R., 1995, Publ. Astron. Soc. Japan 47, 195

Hirata R., Kogure T., 1976, Publ. Astron. Soc. Japan 28, 509

Horn J., Harmanec P., 1973, Folia Fac. Sci. Nat. Univ. Purkyně Brunensis 14 (Physica 13), 71

Horn J., Hubert A.-M., Hubert H., Koubský P., Bailloux N., 1992, A&A 259, L5

Horn J., Koubský P., Hadrava P., Juza K., Kříž S., Škoda P., Štefl S., 1994, A&AS 105, 119

Horn J., Kubát J., Harmanec P. et al., 1996, A&A 309, 521

Hubeny I., Lanz T., 1995, ApJ 439, 875

Hubert H. 1971, A&A 11, 100

Hubert-Delplace A.-M., Hubert H., 1979, An Atlas of Be Stars, Paris-Meudon Observatory

Koubský P., Horn J., Harmanec P., Hubert A.-M., Hubert H., M. Floquet, 1993, A&A 277, 521

Koubský P., Harmanec P., Horn J. et al., 1994, in: Pulsation, rotation and mass loss in early-type stars, IAU Symp. 162, eds. L.A. Balona, H.F. Henrichs & J.M. Le Contel, Kluwer Academic Publishers, p. 370

Kříž S., 1982, Bull. Astron. Inst. Czechosl. 33, 302

Kubát J., 1994, A&A 287, 179

Kubát J., 1996, A&A 305, 255

Kubát J., 1997, A&A 326, 277

Kurucz R.L., 1993, Solar Abundance Model Atmospheres, Kurucz CD-ROM No.19

Landis H.J., Lovell H.P., Hall D.S., Uckotter D.G. 1977, Acta Astron. 27, 265

Ljunggren B, Oja T., 1964, Ark. Astron. 3, 439

Mohler O., 1940, ApJ 92, 315

Müller G., Kempf P., 1907, Publ. Astrophys. Obs. Potsdam 17, 1

Papoušek J., 1979, Scripta Fac. Sci. Nat. UJEP Brunensis, Physica 2 Vol. 9, 75

Pavlovski K., Harmanec P., Božić H. et al., 1997, A&AS, in press

Percy J.R., Attard A., 1992, PASP 104, 1160

Percy J.R., Coffin B.L., Drukier G.A. et al., 1988, PASP 100, 1555

Perryman M.A.C., Høg E., Kovalevsky J., Lindegren L., Turon C., 1997, The Hipparcos and Tycho Catalogues, ESA SP-1200

Pickering E.C., 1884, Harvard Annals 14, 1

Pickering E.C., 1899, Harvard Annals 44, 1

Pickering E.C., 1908, Harvard Annals 50, 1

Plaskett J.S., Harper W.E., Young R.K., Plaskett H.H., 1922, Publ. Dom. Astrophys. Obs. Victoria 1, 287

Pogodin M.A., 1997, A&A 317, 185

Popper D.M., 1980, ARA&A 18, 115

Schuster W.J., Alvarez M. 1983, PASP 95, 35

Škoda P., 1996, in Astronomical Data Analysis Software and Systems V, eds. G.H. Jacoby & J. Barnes, A.S.P. Conference Series, Vol. 101, ASP, San Francisco, p. 187

Vondrák J., 1969, Bull. Astron. Inst. Czechosl. 20, 349

Vondrák J., 1977, Bull. Astron. Inst. Czechosl. 28, 84